

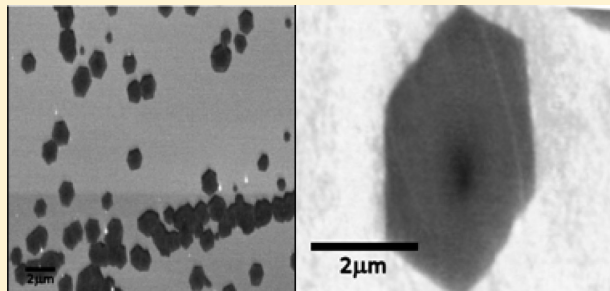
Hexagonal Single Crystal Domains of Few-Layer Graphene on Copper Foils

Alex W. Robertson and Jamie H. Warner*

Department of Materials, University of Oxford, Parks Road, Oxford, OX1 3PH, United Kingdom

 Supporting Information

ABSTRACT: Hexagonal-shaped single crystal domains of few layer graphene (FLG) are synthesized on copper foils using atmospheric pressure chemical vapor deposition with a high methane flow. Scanning electron microscopy reveals that the graphene domains have a hexagonal shape and are randomly orientated on the copper foil. However, the sites of graphene nucleation exhibit some correlation by forming linear rows. Transmission electron microscopy is used to examine the folded edges of individual domains and reveals they are few-layer graphene consisting of approximately 5–10 layers in the central region and thinning out toward the edges of the domain. Selected area electron diffraction of individual isolated domains reveals they are single crystals with AB Bernal stacking and free from the intrinsic rotational stacking faults that are associated with turbostratic graphite. We study the time-dependent growth dynamics of the domains and show that the final continuous FLG film is polycrystalline, consisting of randomly connected single crystal domains.



KEYWORDS: Graphene, chemical vapor deposition, APCVD, CVD

Graphene, a two-dimensional crystal that is the building block of graphite, is an excellent material for electrical applications, such as transparent conducting films, due to the unique nature of its charge carriers.^{1–3} The massless Dirac fermions that constitute the carriers of charge in graphene travel at relativistic speeds and thus exhibit exceptional mobilities with suspended graphene sheets demonstrating carrier mobilities of up to $200\,000\text{ cm}^2\text{ V}^{-1}\text{ s}^{-1}$.⁴ The initial production by the mechanical exfoliation of graphite yielded high quality, micrometer scale graphene flakes that, while ideal for research, were unsuitable for adoption by the industrial sector for applications requiring large area coverage.⁵ The successful synthesis of large area graphene films by chemical vapor deposition on certain metal catalysts, such as nickel and copper,^{6,7} is a major step toward the commercial realization of graphene in products, such as flat panel displays and solar panels.⁸

Studies into the dynamics of CVD graphene growth on copper foils have chiefly focused on monolayer films that develop under vacuum conditions.^{7,9–11} Under these conditions the copper-catalyzed deposition of graphene occurs by a surface adsorption process, rather than a surface segregation followed by precipitation process, as in the case of nickel. This is attributed to the low solubility of carbon in copper, and consequently the growth of graphene on copper is expected to be self-limiting and restricted to that of a single monolayer.⁹ The growth of graphene by low-pressure CVD starts with the nucleation of a large number of domains across the copper surface. These domains form a 4-fold symmetry lobe structure and continue to grow with time until they merge together to form a single sheet of polycrystalline graphene.^{10,11}

A recent study has demonstrated an apparent change in growth kinetics when the deposition pressure is raised to atmospheric pressure with few-layer graphene formed,¹² and a further study yielded bilayer graphene growth on copper.¹³ Both of these studies demonstrate that the previously observed self-limiting growth of graphene on copper does not apply under all synthesis conditions. To our knowledge, the details of the time-dependent growth mechanisms of the domains of few layer graphene have not been thoroughly investigated. Furthermore, information on the crystallinity of the few layer graphene is lacking, which is vital for understanding the band structure, and ultimately the electrical properties of graphene films. Here, we investigate the growth of few-layer graphene by CVD on copper foils at atmospheric pressure primarily using a combination of scanning electron microscopy (SEM) and transmission electron microscopy (TEM) along with selected area electron diffraction (SAED).

Graphene was synthesized by copper-catalyzed chemical vapor deposition under atmospheric pressure, using methane as the carbon containing precursor gas. The method is based upon ref 7; in brief, a hydrogen/argon gas mix (25% hydrogen) was allowed to flow across the copper at a temperature of 1000 °C, where it was annealed and reduced for 30 min. A methane/argon gas mixture (20% methane) of flow rate varying from 10–50 sccm as desired, was then supplied, while

Received: November 28, 2010

Revised: January 27, 2011

Published: February 15, 2011

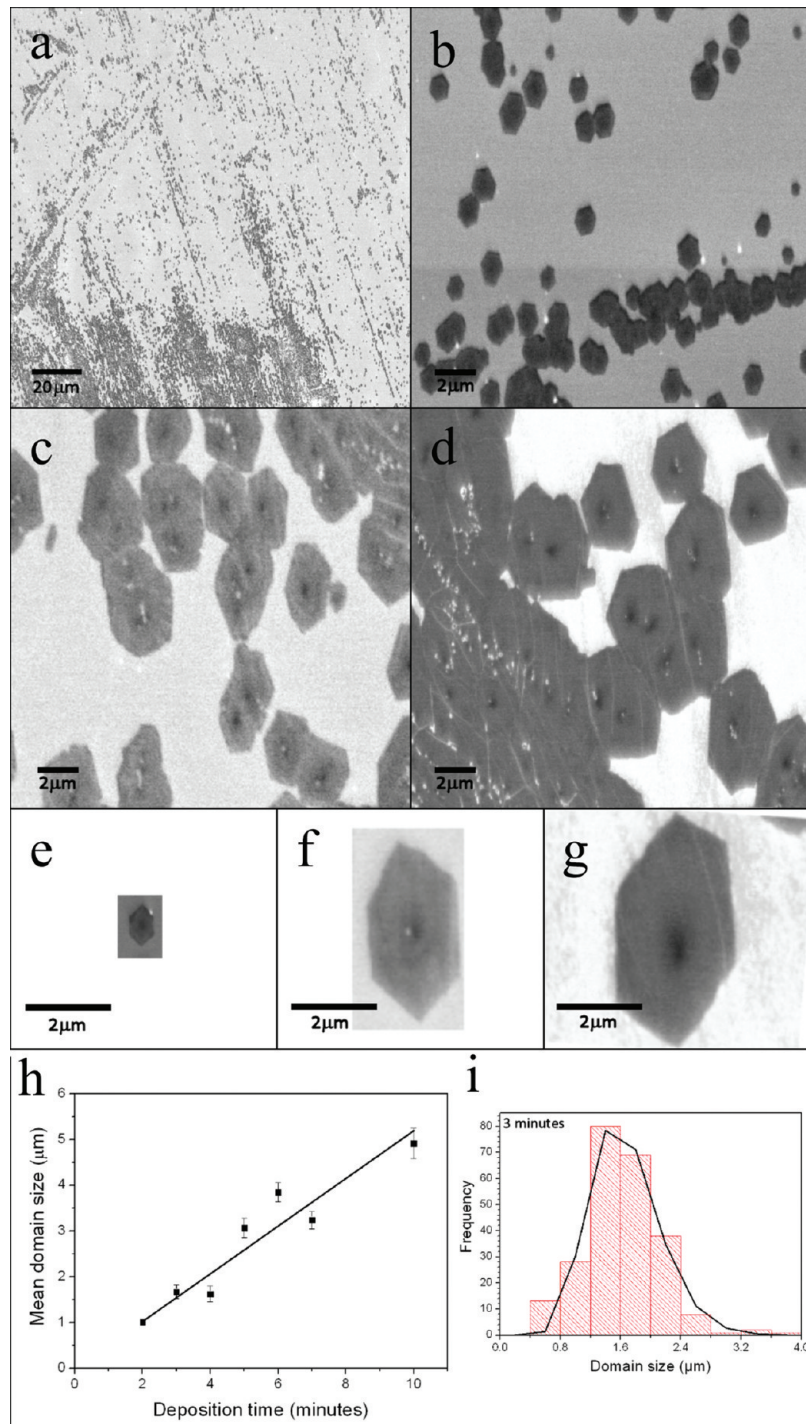


Figure 1. (a) A low magnification image from the 2 min deposition showing a typical distribution of the graphene domains (dark contrast) on the copper foil (bright contrast). (b–d) High-magnification images of 3, 6, and 10 min growths, respectively. (e–g) High-magnification, cropped images showing the relative scale of graphene domains for 3, 6, and 10 min, respectively. (h) The mean graphene domain size with respect to deposition time with the mean determined by a gamma distribution of the distribution of domain sizes, as shown for the 3 min deposition case in (i).

maintaining the 600 sccm hydrogen gas mix flow. The precursor supply time was varied, such that a cross section of graphene growth could be analyzed with respect to growth time. The sample was left to rapidly cool under a hydrogen and argon atmosphere. Analysis by SEM, Raman spectroscopy, and atomic force microscopy (AFM) was conducted directly on the as-grown graphene on copper foil; however, characterization by

TEM required transfer to a TEM grid. A similar method was employed to that outlined in ref 14 with poly(methyl methacrylate) (PMMA) used as a supportive scaffold on the graphene surface while the underlying copper was etched by an iron(III) chloride solution.

An SEM was used to obtain images of the graphene domains directly on the surface of the copper foils without any processing.

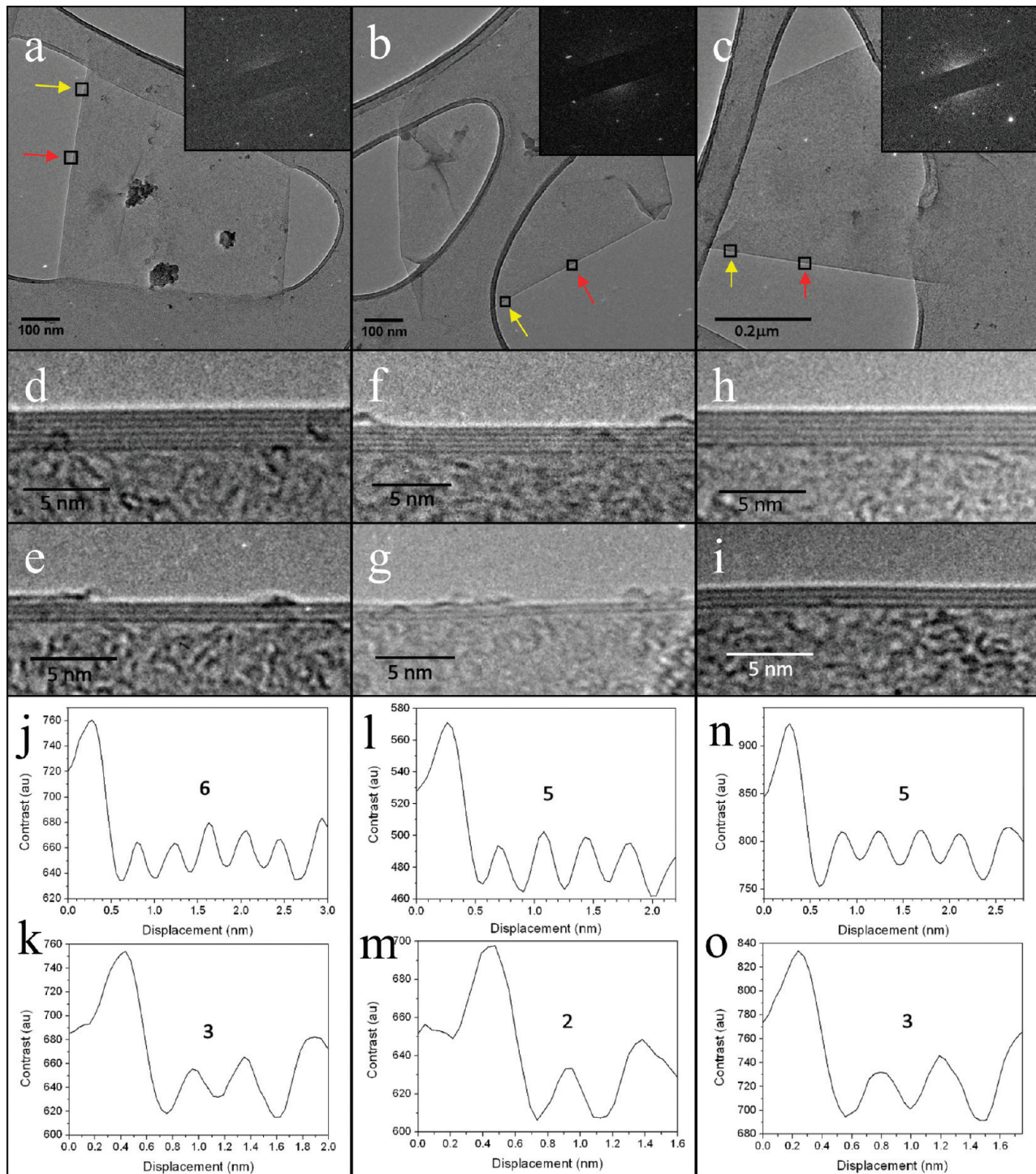


Figure 2. (a–c) TEM images of single, isolated domains of few layer graphene. SAED taken from the center of the domains are shown in the insets. (d–i) HRTEM images of the folds from the arrowed regions in (a–c) with (d,f,h) denoted by the red arrows, and (e,g,i) denoted by the yellow arrows. (j–o) Intensity profiles taken by a box average across an appropriate section of the folded region shown in (d–i) with (j) corresponding to (d), (k) corresponding to (e), and so forth. The number of minima denotes the layer count and is shown above the profile.

This permitted visualization of the shape and location of the graphene domains. A series of graphene depositions on the copper foils were conducted at incremental time intervals of 2, 3, 4, 5, 6, 7, and 10 min with a 20%-methane/argon precursor flow rate of 10–15 sccm. Figure 1a shows a low-magnification image of the copper surface for the 2 min deposition. The areas of dark contrast are graphene domains that have formed on the

bright copper surface. It is apparent from the image that the graphene preferentially nucleates along linear axes, which could be due to the initial graphene nucleation occurring more frequently at step edges, folds, or other imperfections in the copper foil that are linear in character. Figure 1b–d shows images taken at higher magnification for depositions of 3, 6, and 10 min, respectively. The domain shape of the graphene

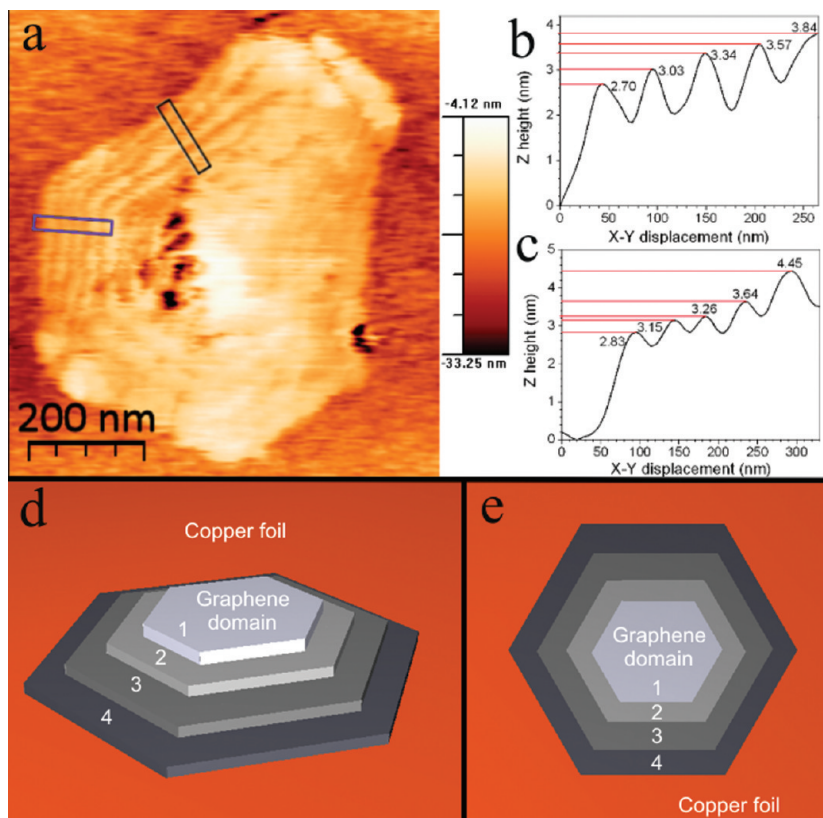


Figure 3. (a) A contact mode AFM image of a FLG domain, scanned from left to right. (b,c) Box-averaged z -height line profiles shown for the black (b) and blue (c) highlighted regions in (a). (d) A 3D schematic representation of a terraced few layer graphene domain on copper foil. (e) Overhead view of a schematic representation of a single terraced, few layer graphene domain on copper foil.

islands can be seen to be hexagonal with individual domains growing into adjacent domains with time. Figure 1e–g shows magnified domains for 3, 6, and 10 min, respectively, and also shows the relative increase in domain size. The hexagonal shape remains for the full range of domain sizes imaged and is not deformed by growth. Size distribution histograms for the graphene domains were constructed with the size of the domain defined as the longest distance between two opposite vertices. It was found that a gamma distribution provided a good fit to the distribution of the domain sizes and could be used to determine their mean size. Figure 1h shows a plot of deposition time versus average domain size, which shows a strong linear correlation and a growth rate of approximately $0.5 \mu\text{m}$ per minute, or an area growth rate of $0.16 \mu\text{m}^2/\text{min}$. Further work was carried out to determine if there was any correlation in the relative angular orientations of the grains; however no noteworthy trends were found (see Supporting Information for details).

TEM was performed on graphene samples that were exposed to a methane flow of 10–15 sccm 20%-methane/argon gas mix precursor for 1 and 3 min. Figure 2a–c shows three typical individual isolated domains from the 1 min exposure to methane. Each of these domains is well separated from other domains and enables the structure of a single domain to be elucidated without the interference of overlapping. The insets in Figure 2a–c show their respective SAED patterns taken from the central region of the domain with care taken to avoid regions that contain back-folded edges. We found that all SAED patterns could be indexed to single crystals of AB Bernal-stacked graphite with only six spots of reflection being observed in the inner hexagon of 0.21

nm spacing. The presence of rotational stacking faults that are typical in turbostratic graphite or poor quality flake graphite leads to extra sets of spots appearing in the SAED patterns, which were not observed in any of the isolated single domains.¹⁵ This demonstrates that the domains are not turbostratic in configuration but in general are well-ordered single crystals. Contrast from the folded edges of graphene is observed in all three imaged domains in Figure 2. The domains are often folded along their edges and no longer display the characteristic hexagonal shape observed in the SEM images. Contrast from the folded edges can be used to reliably characterize the number of graphene layers at that location in the same way that the number of walls in a carbon nanotube can be determined.¹⁶ Figure 2d,e shows the HRTEM images of the folded edges from the regions indicated with a red and yellow arrow, respectively, in Figure 2a. Figure 2d shows six lines of contrast, confirmed by the line profile taken perpendicular to the edge, shown in Figure 2j, indicating that there are six layers of graphene in this region. Moving further along the edge (Figure 2e) results in fewer lines of contrast, which suggests a reduction in the number of graphene layers toward the perimeter of the domain. In Figure 2e, the transition from four layers of graphene to three is apparent. Figure 2f,g shows a similar effect of thinning toward the edges for the domain in Figure 2b, and Figure 2h,i shows it for the domain in Figure 2c. This effect was observed for all edges and indicates the central part of the domain contains more layers than the outer regions. This indicates that the number of graphene layers diminishes closer to the graphene grain boundary in a step pyramid type structure.

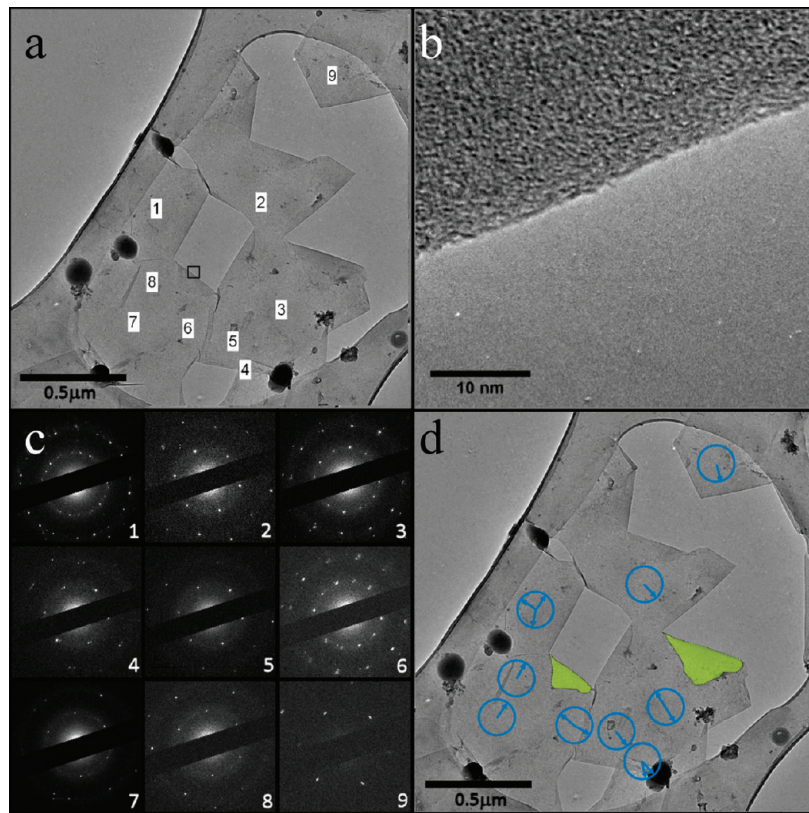


Figure 4. (a) TEM images of several graphene domains in the process of merging together. (b) HRTEM taken from the boxed region shown in (a). (c) SAED of the numbered areas in (a). (d) A polar representation of the relative angular rotation of the SAED patterns from the vertical. In addition, two areas where the shadow of an underlying fold of graphene can be seen are highlighted.

To investigate the thickness of the graphene domains on the copper foil, AFM was used. A contact-mode AFM image of the domain from the 3 min deposition is shown in Figure 3a with the scanning direction from left to right. Line profiles to measure the height as a function of distance were taken across the two regions indicated with boxes in Figure 3a and are shown in Figure 3b,c. The total height of the domain with respect to the copper substrate was found to be approximately 4 nm, significantly greater than the 1–1.6 nm measured for a monolayer film on silicon dioxide,² suggesting FLG. The interlayer spacing in graphite is approximately 3.35 Å; however one must also take into account the effect of the van der Waals force, the substrate-graphene spacing, wetting, and other surface interactions at these high resolutions.¹⁷ These effects act to increase the apparent thickness of a graphene layer on a generic substrate; however, measuring the height of graphene on a graphene substrate is known to give more accurate measurements of between 0.3–0.4 nm.^{2,17} Along the left side of the domain, lines of darker contrast are apparent, which coincide with dips in the z-height profile, shown in Figure 3b,c. Taking z-height measurements from the peaks of the line profiles suggests an average height difference between the peaks of ~0.3 nm, which is in good agreement with the known interlayer spacing for graphite layers. This supports the TEM evidence in Figure 2, where the number of layers of graphene increases toward the central region of the domain. Figure 3d shows a 3D schematic representation of a terraced, hexagonal few-layer graphene domain on a copper foil with the top view shown in Figure 3e. The thickness of each graphene layer is not drawn to

scale relative to the size of the domain for clarity of presentation.

Figure 4a shows a TEM image taken from an area where individual graphene domains have nucleated in close proximity to one another and were beginning to merge together. A number of the edges have folded during the transfer to the TEM grid, illustrated by the highlighted area in Figure 4d. Figure 4b shows the TEM image of a section of a back-folded edge, indicated with the boxed region in Figure 4a. No lines of contrast were resolved at this edge, as with the cases shown in Figure 2, indicating that the thickness of this domain is minimal. In this region, four domains have partially merged, leaving a hole in the central region. Selected area electron diffraction was used to map the crystallographic orientation of the merged domains. Figure 4c shows the SAED patterns for each of the respective numbered regions in Figure 4a. Some areas show multiple spots of 0.21 nm spacing in the SAED patterns, such as 1, 3, and 6, indicating that there are rotational stacking faults within the region measured. This is either due to back-folding of edges, intrinsic rotational stacking faults, overlapping domains or from a boundary region where the two domains meet and have different crystallographic orientations. Since the SAED analysis of individual isolated domains, shown in Figure 2, revealed they were single crystals, intrinsic rotational stacking faults can be ruled out and can thus attribute the presence of multiple spots in some of the SAED patterns to the back-folding of edges, overlapping domains, and domain boundaries with disorientation. The relative angles are shown in a polar representation in Figure 4d for clarity with the angle of displacement relative to the vertical shown normalized

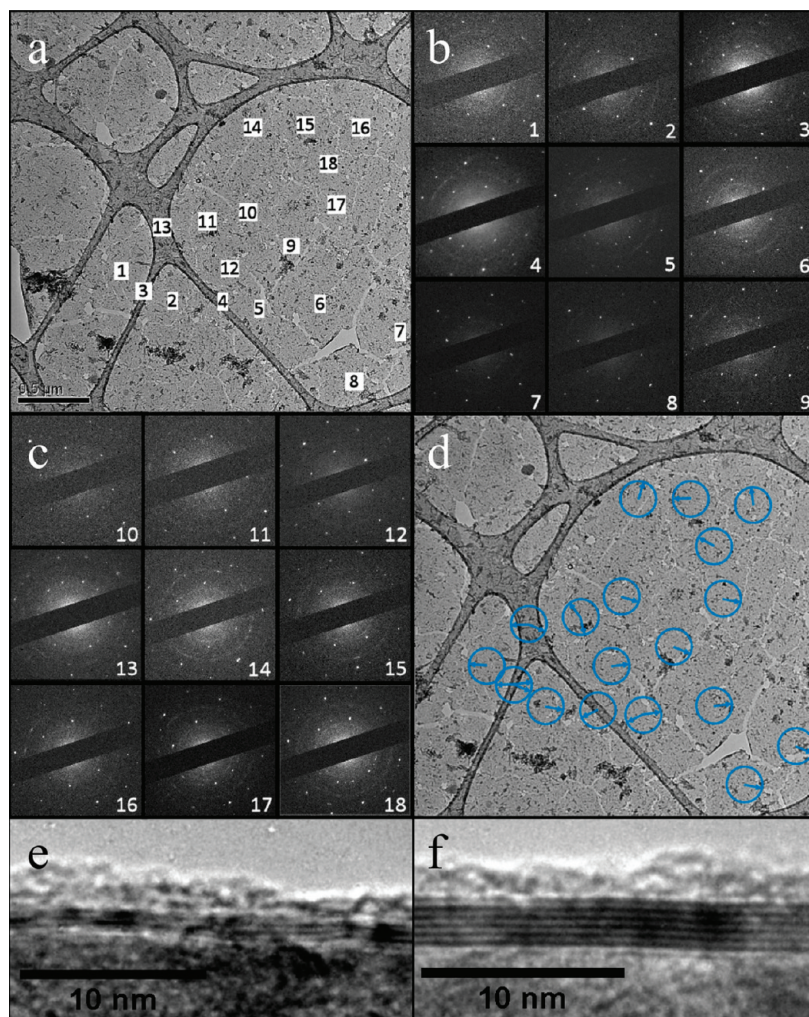


Figure 5. (a) A TEM image of a FLG sheet formed after a 3 min deposition. (b,c) SAED patterns from the appropriately labeled regions in (a). (d) A polar representation of the relative angular rotation of the SAED patterns from the vertical. (e,f) HRTEM images of two folded regions.

to 360° . The SAED patterns of regions 2, 4, 5, and 7–9 in Figure 4c show one set of spots associated with AB Bernal graphite structure, further demonstrating the well-ordered growth of the domains. The angle does not appear to be maintained across adjacent domains; the apparent equivalence of the rotation of regions 7 and 8 with part of region 1 is likely due to the SAED encompassing the adjacent domain with one of the other two diffractions in region 1 attributable to its domain. By examination of the TEM images, it is often discernible that areas that show multiple diffractions are also at, or close to, areas where the shadow of a folded sheet is visible.

As shown in the SEM images in Figure 1, the size of the graphene domains increases with exposure time to methane with several merging to form large macroscopic sheets even after 3 min. Figure 5a shows a TEM image of a large area few-layer graphene sheet on a lacy carbon grid formed from 3 min of methane exposure. Upon the basis of the growth dynamics revealed from the SEM images in Figure 1 and the SAED analysis in Figure 2, we expect this sheet to be polycrystalline and comprised of single crystal domains that have merged together. The 2D maps of the crystallinity of the sheets were obtained by taking SAED patterns, shown in Figure 5b,c, for 18 different regions, labeled in Figure 5a. A high proportion of the regions

measured, 14 out of the 18, showed single crystal SAED patterns, but the relative orientation of the single crystals varied substantially. In Figure 5d, arrows are used to indicate the relative crystallographic direction as determined from the respective SAED pattern. Regions containing two sets of spots in the SAED pattern were attributed to domain boundaries. For example, the SAED patterns from regions 4 and 6 indicate two single crystal domains with different orientation, and the SAED taken in between, region 5, is a superposition of the two patterns seen in regions 4 and 6, suggesting that the grain boundary passes through there. The orientation of the domains appears to be random and no correlations can be observed. HRTEM images of folded regions (Figure 5e,f) demonstrate that there is no appreciable increase in layer number from the shorter growth time case.

Raman spectroscopy is a frequently used technique to characterize graphene.^{18,19} Identifiable peaks are the G peak at $\sim 1580 \text{ cm}^{-1}$, a radial C–C stretching mode associated with sp^2 bonded carbon; the D peak at $\sim 1350 \text{ cm}^{-1}$, a first order zone boundary phonon mode associated with defects in the graphene or graphene edges; and the 2D peak at $\sim 2700 \text{ cm}^{-1}$, a second order zone boundary phonon mode associated with graphene and graphite. Figure 6 shows representative Raman spectra from

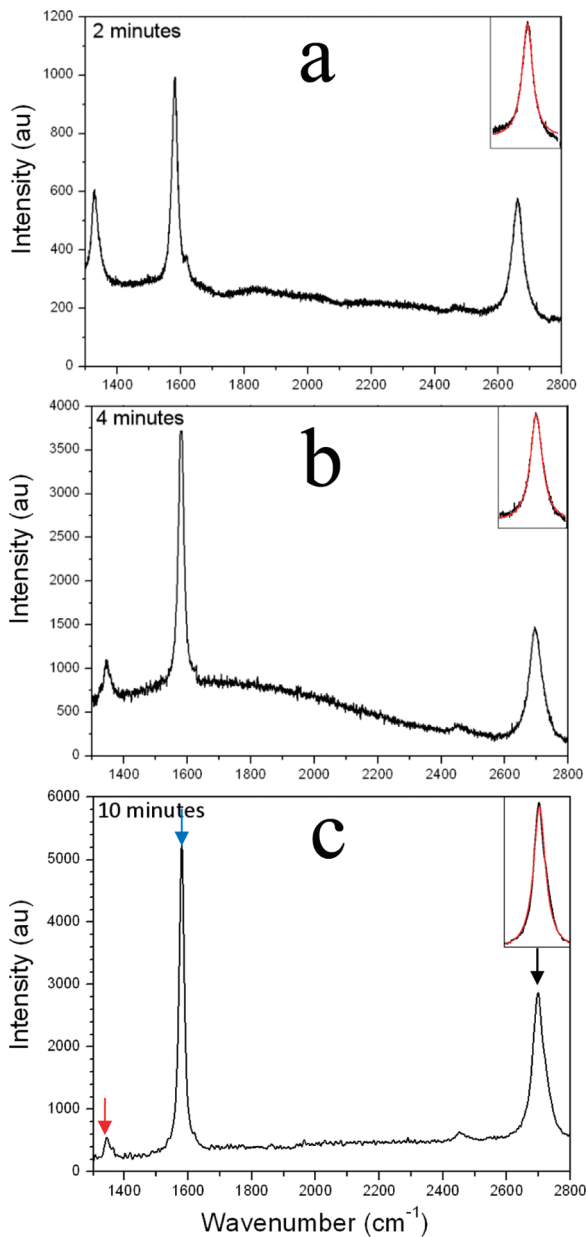


Figure 6. Raman spectra for graphene grown on copper foil for (a) 2, (b) 4, and (c) 10 min deposition. Copper signal subtracted, taken with a S32 nm wavelength laser. The red arrow corresponds to the D-peak and occurs at 1345 cm^{-1} , the blue arrow is the G peak at 1580 cm^{-1} , and the black arrow is the 2D peak at 2700 cm^{-1} . The insets shows a single Lorentzian (red) profile fitted to the 2D peaks (black); see Tables S1–S3 (Supporting Information) for fit data.

graphene grown on copper for (a) 2, (b) 4, and (c) 10 min deposition times. The copper foil background signal was subtracted for clarity. The G and 2D peaks at the blue and black arrows, respectively, confirm the presence of graphitic carbon. The weak D peak suggests some disorder, but a D/G ratio of 0.11–0.46 is comparable with few layer graphene films prepared using Ni substrates.²⁰ The Raman spectra in Figure 6 also show that the D/G ratio decreases as the growth time increases. We attribute this to the increase in the domain size of the graphene with time and the reduction of the contribution of the edges to the overall Raman signal. Analysis of the 2D peak can be used to

determine the layer count of graphene with a monolayer yielding a peak that can be fitted by a single Lorentzian line shape.¹⁸ However, this may also be attributable to turbostratic graphene, where the full-width half-maximum (fwhm) of the peak is roughly double that for the monolayer case ($\text{fwhm} \approx 50\text{ cm}^{-1}$) along with an upshift of $\sim 20\text{ cm}^{-1}$.¹⁸ The 2D peaks shown in Figure 6 were fitted with single Lorentzian profiles with fwhms of 41.9 ± 0.3 , 49.0 ± 0.4 , and $46.5 \pm 0.5\text{ cm}^{-1}$, for 2, 4, and 10 min, respectively. In the absence of other characterization techniques, this would suggest turbostratic graphene was grown on the copper foil. However, the combination of SEM, TEM, AFM, and SAED has provided us with in-depth knowledge of the structure of the few-layer graphene material synthesized and conclusively rules out the formation of extensive amounts of turbostratic graphene. This indicates that the presence of a broadened, single Lorentzian 2D peak is not always interpretable as corresponding to turbostratic graphene. This agrees with the results of Reina et al., who found the profile of the 2D peak in the Raman spectra from few layer graphene grown by CVD on Ni surfaces also broadens to a single peak.²⁰ They found that the ratio of the intensity of the G peak, I_G , to the 2D peak, I_{2D} , correlates with the layer number. The ratio of I_G/I_{2D} increases as the number of layers increases with a value greater than 1 indicative of more than one layer. For three layers of graphene, Reina et al. reported a ratio of $I_G/I_{2D} = 1.3$ with a fwhm of 70 cm^{-1} .²⁰ We find from Figure 6 a ratio I_G/I_{2D} of 1.8, 2.4, and 1.9, which indicates more than 3 layers, however the fwhm of approximately 45 cm^{-1} is substantially less than the 70 cm^{-1} reported by Reina et al.²⁰ This highlights that care is required when relying solely upon Raman spectroscopy to determine the number of layers of CVD grown graphene.

The hexagonal shape of the graphene domains are dissimilar to the four-lobed structures that have been found elsewhere for graphene grown on copper foil.^{10,11} Furthermore, the tendency for the graphene to form into AB Bernal few-layer stacks, as opposed to a monolayer film, suggests that the graphene deposition is not a simple surface catalyzed process for the experimental conditions studied here. Wofford et al. attribute the formation of the four-lobed structures to the copper and the graphene both affecting the growth configuration due to the 2-fold symmetry that is observed.¹⁰ Here, the hexagonal structures have a 6-fold symmetry, suggesting a growth mechanism that is dominated by the graphene structure with little influence from the underlying copper catalyst. The growth of graphene layers on the top surface of the underlying graphene further demonstrates the lack of importance of the copper catalyst in this regime; the graphene here is growing with no contact with the copper surface. Few-layer graphene growth is known to occur for Ni-catalyzed graphene growth; however, this is due to the high-temperature dependence of carbon solubility in the nickel case, leading to surface segregation followed by precipitation on cooling. The lack of large area monolayer coverage due to surface segregation, coupled with the low solubility of carbon in copper, even at elevated temperatures, would tend to rule out a similar mechanism occurring here. The formation of few-layer graphene seems to occur at an early stage, with little to no observation of monolayer graphene identified from fold fringes in TEM analysis. This is potentially due to particularly high supersaturation of carbon precursor at the copper/graphene surface due to the high methane flow rates used compared to low pressure deposition. However, the higher pressures used here would act to counter this, reducing the reactant diffusion rate through the boundary

layer and thus lowering the precursor saturation at the surface. As shown by Bhaviripudi et al.,¹² the high pressure is insufficient to overcome the excess in precursor supply in all but the most supply-limited cases, where it was found that reduction of precursor supply to the parts per million regime was needed to induce monolayer deposition at the high atmospheric pressure. Hence, it is reasonable to conclude that the few-layer graphene growth occurs due to particularly high levels of precursor supersaturation due to excess precursor supply. An argument against this is the low graphene growth rate of $\sim 0.2 \mu\text{m}^2$ per minute, whereas considerably higher growth rates of up to $100 \mu\text{m}^2$ per minute are observed for low-pressure growth by Li et al.¹¹ Higher precursor supersaturation should lead to considerably faster graphene growth, and this is not observed. One could hypothesize that the lower growth rate is due to the increase in reactant quantity required in the shift from the monolayer to few-layer growth regime; however, assuming a linear dependence for precursor requirement with layer count, one would not still expect such a marked difference as the several orders of magnitude seen here. It is possible that impurities, such as oxygen, may play a role in etching the edges of the graphene as it forms, leading to the hexagonal domains observed. However, it is difficult to envisage a situation where sufficient impurities would be present to etch all of the vast number of domains that form simultaneously.

In summary, single crystal domains of few-layer graphene have been grown by atmospheric pressure chemical vapor deposition on a copper catalyst. The individual domains have been verified to be AB Bernal stacked crystals by SAED and form into a characteristic hexagonal shape, likely stemming from the crystal symmetry of graphene. Subsequent graphene layers not in contact with the copper surface appear to grow in terraces from the center of the domain, as demonstrated by both contact AFM and HRTEM. The absence of self-limited monolayer graphene growth suggests a different growth mechanism is possible on a copper catalyst under high precursor supply conditions, which while resulting in few-layer graphene, still maintains high quality crystallinity within the domain.

■ ASSOCIATED CONTENT

S Supporting Information. Method details, additional SEM images and data, Raman spectra fit data and equipment information. This material is available free of charge via the Internet at <http://pubs.acs.org>.

■ AUTHOR INFORMATION

Corresponding Author

*E-mail: Jamie.warner@materials.ox.ac.uk.

■ ACKNOWLEDGMENT

J.H.W. thanks the Royal Society and Brasenose College, Oxford for support.

■ REFERENCES

- (1) Novoselov, K. S.; Geim, A. K.; Morozov, S. V.; Jiang, D.; Katsnelson, M. I.; Grigorieva, I. V.; Dubonos, S. V.; Firsov, A. A. Two-dimensional gas of massless Dirac fermions in graphene. *Nature* **2005**, *438*, 197–200.
- (2) Novoselov, K. S.; Geim, A. K.; Morozov, S. V.; Jiang, D.; Zhang, Y.; Dubonos, S. V.; Grigorieva, I. V.; Firsov, A. A. Electric field effect in atomically thin carbon films. *Science* **2004**, *306*, 666–669.

(3) Novoselov, K. S.; Morozov, S. V.; Mohinddin, T. M. G.; Ponomarenko, L. A.; Elias, D. C.; Yang, R.; Barbolina, I. I.; Blake, P.; Booth, T. J.; Jiang, D.; Giesbers, J.; Hill, E. W.; Geim, A. K. Electronic properties of graphene. *Phys. Status Solidi B* **2007**, *244* (11), 4106–4111.

(4) Bolotin, K. I.; Sikes, K. J.; Jiang, Z.; Klima, M.; Fudenberg, G.; Hone, J.; Kim, P.; Stormer, H. L. Ultrahigh electron mobility in suspended graphene. *Solid State Commun.* **2008**, *146* (9–10), 351–355.

(5) Novoselov, K. S.; Jiang, D.; Schedin, F.; Booth, T. J.; Khotkevich, V. V.; Morozov, S. V.; Geim, A. K. Two-dimensional atomic crystals. *Proc. Natl. Acad. Sci. U.S.A.* **2005**, *102* (30), 10451–10453.

(6) Kim, K. S.; Zhao, Y.; Jang, H.; Lee, S. Y.; Kim, J. M.; Kim, K. S.; Ahn, J. H.; Kim, P.; Choi, J. Y.; Hong, B. H. Large-scale pattern growth of graphene films for stretchable transparent electrodes. *Nature* **2009**, *457*, 706–710.

(7) Li, X.; Cai, W.; An, J.; Kim, S.; Nah, J.; Yang, D.; Piner, R.; Velamakanni, A.; Jung, I.; Tutuc, E.; Banerjee, S. K.; Colombo, L.; Ruoff, R. S. Large-area synthesis of high-quality and uniform graphene films on copper foils. *Science* **2009**, *324*, 1312–1314.

(8) Bae, S.; Kim, H.; Lee, Y.; Xu, X.; Park, J. S.; Zheng, Y.; Balakrishnan, J.; Lei, T.; Kim, H. R.; Song, Y. I.; Kim, Y. J.; Kim, K. S.; Özyilmaz, B.; Ahn, J. H.; Hong, B. H.; Iijima, S. Roll-to-roll production of 30-in. graphene films for transparent electrodes. *Nat. Nanotechnol.* **2010**, *5* (8), 574–578.

(9) Li, X.; Cai, W.; Colombo, L.; Ruoff, R. S. Evolution of graphene growth on Ni and Cu by carbon isotope labeling. *Nano Lett.* **2009**, *9* (12), 4268–4272.

(10) Wofford, J. M.; Nie, S.; McCarty, K. F.; Bartelt, N. C.; Dubon, O. D. Graphene Islands on Cu Foils: The interplay between Shape, Orientation, and Defects. *Nano Lett.* **2010**, *10* (12), 4890–4896.

(11) Li, X.; Magnuson, C. W.; Venugopal, A.; An, J.; Suk, J. W.; Han, B.; Borysiak, M.; Cai, W.; Velamakanni, A.; Zhu, Y.; Fu, L.; Vogel, E. M.; Voelkl, E.; Colombo, L.; Ruoff, R. S. Graphene Films with Large Domain Size by a Two-Step Chemical Vapor Deposition Process. *Nano Lett.* **2010**, *10* (11), 4328–4334.

(12) Bhaviripudi, S.; Jia, X.; Dresselhaus, M. S.; Kong, J. Role of Kinetic Factors in Chemical Vapor Deposition Synthesis of Uniform Large Area Graphene Using Copper Catalyst. *Nano Lett.* **2010**, *10* (10), 4128–4133.

(13) Lee, S.; Lee, K.; Zhong, Z. Wafer Scale Homogeneous Bilayer Graphene Films by Chemical Vapor Deposition. *Nano Lett.* **2010**, *10* (11), 4702–4707.

(14) Li, X.; Zhu, Y.; Cai, W.; Borysiak, M.; Han, B.; Chen, D.; Piner, R. D.; Colombo, L.; Ruoff, R. S. Transfer of Large-Area Graphene Films for High-Performance Transparent Conductive Electrodes. *Nano Lett.* **2009**, *9* (12), 4359–4363.

(15) Warner, J. H.; Rümmeli, M. H.; Gemming, T.; Büchner, B.; Briggs, G. A. D. Direct Imaging of Rotational Stacking Faults in Few Layer Graphene. *Nano Lett.* **2008**, *9* (1), 102–106.

(16) Meyer, J. C.; Geim, A. K.; Katsnelson, M. I.; Novoselov, K. S.; Booth, T. J.; Roth, S. The structure of suspended graphene sheets. *Nature* **2007**, *446*, 60–63.

(17) Nemes-Incze, P.; Osváth, Z.; Kamarás, K.; Biró, L. P. Anomalies in thickness measurements of graphene and few layer graphite crystals by tapping mode atomic force microscopy. *Carbon* **2008**, *46* (11), 1435–1442.

(18) Ferrari, A. C.; Meyer, J. C.; Scardaci, V.; Casiraghi, C.; Lazzari, M.; Mauri, F.; Piscanec, S.; Jiang, D.; Novoselov, K. S.; Roth, S.; Geim, A. K. Raman spectrum of graphene and graphene layers. *Phys. Rev. Lett.* **2006**, *97*, No. 187401.

(19) Dresselhaus, M. S.; Jorio, A.; Hofmann, M.; Dresselhaus, G.; Saito, R. Perspectives on Carbon Nanotubes and Graphene Raman Spectroscopy. *Nano Lett.* **2010**, *10* (3), 751–758.

(20) Reina, A.; Jia, X.; Ho, J.; Nezich, D.; Son, H.; Bulovic, V.; Dresselhaus, M. S.; Kong, J. Large Area, Few-Layer Graphene Films on Arbitrary Substrates by Chemical Vapor Deposition. *Nano Lett.* **2009**, *9* (1), 30–35.